

Electronically highly cubic conditions for Ru in α -RuCl₃

S. Agrestini,¹ C.-Y. Kuo,¹ K.-T. Ko,¹ Z. Hu,¹ D. Kasinathan,¹ H. Babu Vasili,² J. Herrero-Martin,² S. M. Valvidares,² E. Pellegrin,² L.-Y. Jang,³ A. Henschel,¹ M. Schmidt,¹ A. Tanaka,⁴ and L. H. Tjeng¹

¹Max Planck Institute for Chemical Physics of Solids, Nöthnitzerstr. 40, 01187 Dresden, Germany

²ALBA Synchrotron Light Source, E-08290 Cerdanyola del Vallès, Barcelona, Spain

³National Synchrotron Radiation Research Center, 101 Hsin-Ann Road, Hsinchu 30076, Taiwan

⁴Department of Quantum Matter, ADSM, Hiroshima University, Higashi-Hiroshima 739-8530, Japan

(Dated: June 3, 2021)

We studied the local Ru *4d* electronic structure of α -RuCl₃ by means of polarization dependent x-ray absorption spectroscopy at the Ru-*L*_{2,3} edges. We observed a vanishingly small linear dichroism indicating that electronically the Ru *4d* local symmetry is highly cubic. Using full multiplet cluster calculations we were able to reproduce the spectra excellently and to extract that the trigonal splitting of the *t*_{2g} orbitals is -12 ± 10 meV, i.e. negligible as compared to the Ru *4d* spin-orbit coupling constant. Consistent with our magnetic circular dichroism measurements, we found that the ratio of the orbital and spin moments is 2.0, the value expected for a $J_{\text{eff}} = 1/2$ ground state. We have thus shown that as far as the Ru *4d* local properties are concerned, α -RuCl₃ is an ideal candidate for the realization of Kitaev physics.

PACS numbers: 71.70.Ch, 75.70.Tj, 75.10.Kt, 78.70.Dm, 72.80.Ga

Geometrically frustrated quantum spin systems are important owing to the fact that frustration often results in a suppression of conventional mean field ground states in favor of more exotic phases of matter. Current research focuses on the effect of spin-orbit coupling (SOC) and the role it plays in the realization of different exotic phases such as unconventional superconductivity or quantum spin liquids [1–3]. Especially, quantum spin liquids can result in topological states with fractional excitations. An important, theoretically solvable model is the Kitaev model with spin-1/2 on a honeycomb lattice, where the coupling between neighboring spins is highly anisotropic with bond-dependent spin interactions. In contrast to spin liquids arising from usual geometrical frustrated spin arrangements, the bond-dependent spin interactions within the Kitaev model frustrate the spin configuration on a single site [4].

The search for fractionalized excitations and the identification of a Kitaev spin liquid state has been experimentally quite difficult. Increased attention has been focussed on the honeycomb iridates [5, 6], starting from the assumption that large spin-orbit coupling is the leading energy scale in determining the ground state such that the Ir *5d* *t*_{2g} orbitals are described in terms of $J_{\text{eff}} = 1/2$ and $3/2$ orbitals. However, the real iridate systems exhibit trigonal distortion ($D_{\text{trig}} = 0.1$ eV [6]) and a significant itinerant character of the Ir *5d* orbitals [7–9], which complicates the electronic ground state. Despite a flurry of both theoretical and experimental studies, the nature of the ground state in honeycomb iridates are being fiercely debated and the occurrence of Kitaev physics is still far from clear.

Recently, α -RuCl₃ has been suggested as a promising candidate material for the realization of the Kitaev model [10] and excitations observed via Raman [11, 12] and in-

elastic neutron scattering [13] have been presented as evidence that α -RuCl₃ may be close to a quantum spin liquid ground state. In the last two years a number of publications discussing the realization of the Kitaev physics in α -RuCl₃ has appeared in literature [3, 14–18, 20–35]. α -RuCl₃ has a monoclinic structure, where the Ru atoms are arranged in nearly regular honeycomb planes with a Ru-Cl-Ru bond close to 90°, the latter being one of the conditions for the realization of Kitaev magnetism. The Ru³⁺ ions in α -RuCl₃ (hereafter RuCl₃) have the same *t*_{2g}⁵ configuration as Ir⁴⁺ ions in the iridates. The SOC, despite being modest (~ 150 meV), is still thought to be the leading energy scale and able to generate a $J_{\text{eff}} = 1/2$ ground state.

Unfortunately, a precise determination of the atomic positions of the Cl ions by x-ray diffraction (XRD) is quite difficult with conflicting reports about the crystallographic structure of RuCl₃ [3, 13, 14, 36] in literature due to the broad mosaicity arising from the weak Van-der-Waals bond existing between the layers. The intensity of Bragg peaks in XRD is strongly affected by the diffuse scattering produced by twins and sliding stacking faults. We will refer in the following to the last diffraction study [3], which was performed on untwinned RuCl₃ single crystals with moderate stacking faults. According to this investigation, the local structure is close to cubic despite the low symmetry of the point group of the Ru site, and the dominant distortion of the RuCl₃ octahedra is trigonal with the trigonal axis normal to the *ab* plane. Additional tetragonal distortions are present but negligible [3].

Notwithstanding the moderate trigonal distortion, quantum chemistry calculations using the structure given by Ref. 3 proposed a complete lifting of the degeneracy of the *t*_{2g} orbitals by a trigonal splitting of $D_{\text{trig}} = 70$ meV

[20]. Experimentally, a splitting of the order of the SOC was estimated from the large anisotropy shown by high field magnetization measurements [15]. Raman scattering spectroscopy observed a single peak instead of the two-peak structure characteristic for trigonal distortion, which might indicate a nearly cubic local symmetry but could also be explained with the zero-intensity of one peak for symmetry reasons (e.g. selection rules) [21]. Considering the critical importance of the local symmetry for the realization of the Kitaev physics, there is a clear need to establish in a quantitative way the magnitude of the trigonal distortion and its effect on the magnetic ground state of RuCl_3 . Theoretical studies in the literature have shown that the analysis of the ground state of RuCl_3 heavily relies on the trigonal field strength relative to the SOC [22, 23].

Here, we report on a Ru $L_{2,3}$ edge x-ray absorption spectroscopy (XAS) study of the local electronic and magnetic state of the Ru^{3+} ion in RuCl_3 , using both linear and circular polarized light. In combination with full-multiplet cluster simulations using parameters which are based on *ab-initio* band structure calculations, we can extract values for the trigonal crystal field splitting as well as the ratio between the orbital and spin contributions to the local magnetic moment, thereby evaluating to what extent the local $J_{\text{eff}} = 1/2$ ground state is realized for the Ru ion.

Starting from polycrystalline RuCl_3 (Chempur) the crystals were obtained by chemical transport reaction with chlorine between 730 to 660 °C. The crystals were annealed for five months at 440 °C under vacuum. A full characterization of the crystals is provided in Ref. 16. The linear polarized XAS at the Ru- $L_{2,3}$ edges (2800-3000 eV) was measured at the 16A1 tender x-ray beamline of the NSRRC in Taiwan. The spectra were collected at room temperature in the total electron yield (TEY) mode. The degree of linear polarization of the in-

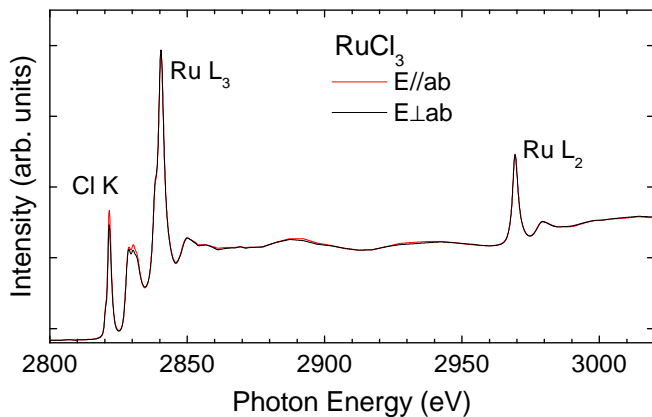


FIG. 1: (color online) Ru- $L_{2,3}$ XAS spectra of a RuCl_3 single crystal for incoming linear polarized light with the electric field vector \mathbf{E} normal (black line) and parallel (red line) to the ab plane.

cident light was close to 100% and the energy resolution was set to 0.6 eV. The x-ray magnetic circular dichroism (XMCD) experiments at the Ru- $L_{2,3}$ edges were performed at the BL29 Boreas beamline of the ALBA synchrotron radiation facility in Barcelona. The energy resolution was 1.4 eV and the degree of circular polarization delivered by the Apple II-type elliptical undulator was set to 70%. The spectra were recorded in the TEY method at $T = 2$ K and $B = 6$ T. The RuCl_3 crystals were cleaved *in situ* to obtain a clean sample surface normal to the (001) direction. Density functional theory (DFT) based calculations were carried out using the full-potential local-orbital code FPLO [37], including both SOC and electron correlation (U) effects for the simplest ferromagnetic spin configuration [38].

In Fig. 1 we report the Ru- $L_{2,3}$ XAS measured on RuCl_3 at room temperature for linearly polarized light coming in with the electric field vector \mathbf{E} normal and parallel to the ab -plane. The chosen geometry has the incoming light polarization parallel and normal to the trigonal axis [111] of the local D_{3d} symmetry. The Ru $2p$ core-hole spin-orbit coupling splits the spectrum roughly in two parts, namely the L_3 (at $h\nu \approx 2840$ eV) and the L_2 (at $h\nu \approx 2969$ eV) white line regions. Additional features appearing in the low energy part of the spectrum are related to the Cl- K edge at $h\nu \approx 2822$ eV.

We first focus on the Cl- K edge features, which can be explained in terms of dipole allowed transitions from the Cl $1s$ core level to the unoccupied Cl $3p$ states. Fig. 2 displays the Cl $3p$ and Ru $3d$ partial density of states (DOS) from the DFT calculations, which reveal the pres-

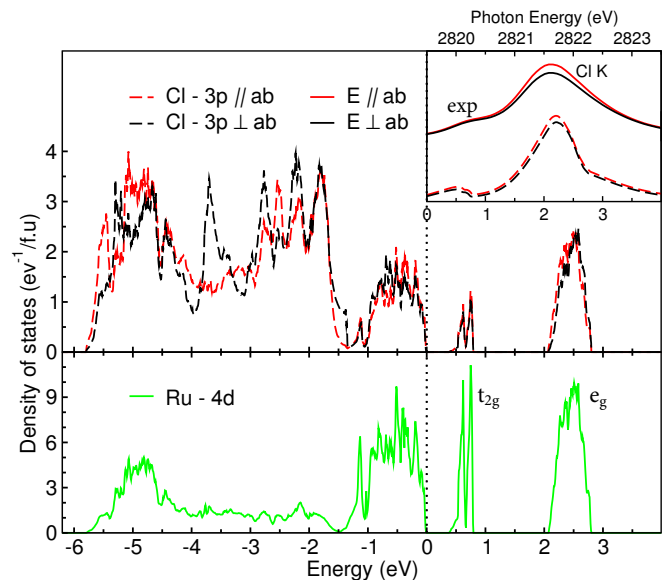


FIG. 2: (color online) Partial density of states of the Cl- $3p$ orbitals for different polarization (top) and of the Ru- $4d$ orbitals (bottom). The inset compares the broadened unoccupied DOS of Cl- $3p$ to the Cl- K edge of the measured XAS spectra.

ence of two sharp features above the Fermi level, namely at ~ 0.5 eV and ~ 2.4 eV. These are given by the unoccupied Ru $4d$ t_{2g} and e_g states, respectively, hybridizing with the Cl $3p$. Comparing these unoccupied Cl states with the experimental Cl- K edge features, we can observe a very satisfactory agreement, especially when we include a broadening for the calculated curves in order to take the experimental resolution into account. Also the weak but clear polarization dependence in the experimental spectra is well explained by the DFT calculations.

For a better view of the multiplet and polarization dependence in the Ru- $L_{2,3}$ spectra we show in Fig. 3 a close-up of the spectra. Notably there is hardly any linear dichroism (LD) visible at the low energy peak (at 2838 eV) of the L_3 edge, which corresponds to the signal of the t_{2g} orbitals. The absence of LD is a very sensitive signal for how close to cubic the local symmetry is. For example, a trigonal elongation (compression) of the RuCl_6 octahedron will cause a splitting of the t_{2g} orbitals into a_{1g} and e_g^π orbitals, with the a_{1g} orbital lying higher (lower) in energy and, hence, having more (less) holes. Such an uneven hole distribution will then produce a difference in the spectral weight between \mathbf{E} normal and parallel to the $[111]$ axis. The experimental result that the LD is vanishingly small gives a clear and direct indication that the trigonal distortion of the RuCl_6 octahedra is electronically negligible.

To obtain a quantitative estimate of how close to cubic the system is from an electronic point of view, we have simulated the Ru- $L_{2,3}$ XAS spectrum using the configuration-interaction cluster model [39, 40]. This model includes the full atomic multiplet theory and takes into account the intra-atomic $4d-4d$ and $2p-4d$ Coulomb interactions, the atomic $2p$ and $4d$ spin-orbit couplings, the Cl- $3p$ with Ru- $4d$ hybridization, and the local crystal field parameters. In the simulations we considered a RuCl_6 cluster with a D_{3d} symmetry as further distortions of the octahedra beyond the trigonal symmetry can be safely neglected [3, 14]. The cubic crystal field splitting between the Ru t_{2g} and e_g orbitals was estimated from the difference in energy position between the maximum in the XAS spectrum, corresponding to the signal from the unoccupied e_g levels, and the maximum of the XMCD signal (see below), which is due to the t_{2g} orbitals. The hybridization parameters and the crystal field acting on the chlorine ligands were extracted *ab-initio* by DFT calculations. The calculations of the XAS spectra were performed using the XTLS 8.3 code [41] and the input parameters are given in Ref. 42.

The calculated Ru- $L_{2,3}$ XAS spectra are plotted in Fig. 3(a). They nicely reproduce the experiment. In order to show how the trigonal distortion affects LD, we have plotted in Fig. 3(b) the experimental difference spectrum ($\mathbf{E}_{\perp ab} - \mathbf{E}_{\parallel ab}$) together with the calculations for different trigonal crystal field splitting $D_{\text{trig}} = E(e_g^\pi) - E(a_{1g})$. As one can see, the LD is very sensitive to the mag-

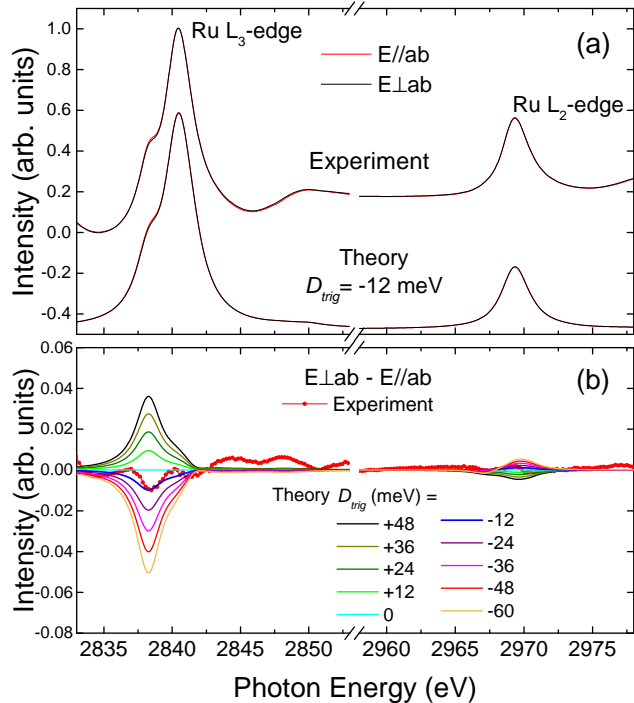


FIG. 3: (color online) (a): Close-up of the Ru- $L_{2,3}$ XAS spectra of a RuCl_3 single crystal for incoming linear polarized light with the electric field vector \mathbf{E} normal (black lines) and parallel (red lines) to the ab plane. (b): Experimental difference spectrum (red circles) compared with calculations for different values of D_{trig} .

nitude and sign of the trigonal splitting. For positive D_{trig} , the calculated LD has the opposite sign compared to the experimental one. On the other hand, a negative $D_{\text{trig}} = -24$ meV produces a LD signal with the correct sign but is already twice as large compared to the experiment. Hence, our experimental LD signal provides strong limits for the trigonal splitting of the t_{2g} orbitals. The best fit to the experimental data is obtained for $D_{\text{trig}} = -12$ meV. The accuracy of our method is actually limited by the presence of the Cl K -edge EXAFS oscillations which occur in the same region as the Ru- $L_{2,3}$ edges. Part of these EXAFS oscillations show up as a slow varying background outside the Ru L -edge white line region (Fig. 3(b)) and is as small as the small LD in the Ru- $L_{2,3}$. Thus, our estimates result in a $D_{\text{trig}} = -12 \pm 10$ meV. This is an important finding since we now can conclude that the trigonal crystal field splitting is at least ten times smaller than the spin-orbit coupling constant (~ 150 meV), implying that the Ru d^5 ion may indeed be in the $J_{\text{eff}} = 1/2$ ground state.

Having established the crystal field situation, we now investigate the magnetic ground state of the Ru ions by performing Ru- $L_{2,3}$ x-ray absorption measurements us-

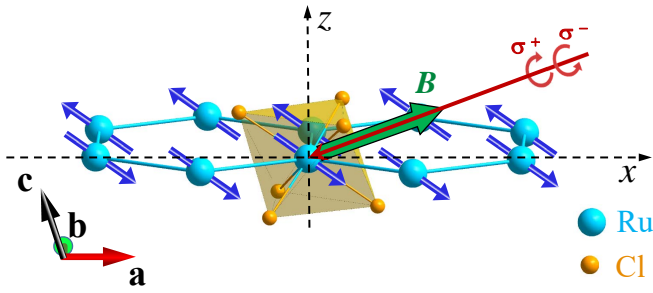


FIG. 4: (color online) Setup of the XMCD experiment: the magnetic field B is applied parallel to the Poynting vector of the circularly polarized photons and forms an angle of 20° with the ab plane.

ing circular polarized light with the photon spin aligned parallel (σ^+) and antiparallel (σ^-) to the magnetic field. A sketch of the experimental geometry is shown in Fig. 4. The difference or XMCD spectrum ($\sigma^+ - \sigma^-$) and the sum spectrum ($\sigma^+ + \sigma^-$) are reported in Fig. 5. The spectra were collected at $T = 2$ K in grazing incidence with the magnetic field ($B = 6$ T) lying in the ac plane (xz plane in local D_{3d} symmetry) and forming an angle of 20° with the (100) axis (x -axis in local symmetry). The grazing geometry allowed to maximize the magnetic signal according to the easy-plane magnetic anisotropy of RuCl_3 reported in literature [15, 16].

The $\text{Ru-}L_{2,3}$ XMCD spectrum as obtained from our full-multiplet calculations is also presented in Fig. 5. In our model we have used the same parameters as for the simulation of the LD data, with $D_{trig} = -12$ meV. The lineshape of the calculated XMCD spectrum is in nice agreement with the experimental one, further validating our calculations. Here, we have used an exchange field of about $H_{ex} = 10$ meV in order to reproduce the magnitude of the experimental XMCD spectrum. If we would have used zero exchange field, the calculated XMCD signal in an applied field of 6 Tesla is much larger than the measured one, i.e. the magnitude of the XMCD is very sensitive to the size of the exchange field (see supplemental information). This in fact can be understood as RuCl_3 exhibits a zig-zag modulated antiferromagnetic order below $T_N = 8$ K and the XMCD signal is given only by the canting of the moments induced by the applied field. The exchange field we have applied is directed along the Ru spins, which form an angle of $\phi = 35^\circ$ with the ab plane [3] (blue arrows in Fig. 3). We would like to note that the XMCD alone is rather unsuitable to determine accurately the magnitude of the trigonal crystal field splitting (see supplemental information).

Having obtained D_{trig} from LD and H_{ex} from XMCD we can now focus on the orbital moment of Ru in RuCl_3 . Very interestingly, the XMCD signal has the same negative sign at both L_3 and L_2 edges. Usually, the XMCD has the opposite sign at the two edges, which is a con-

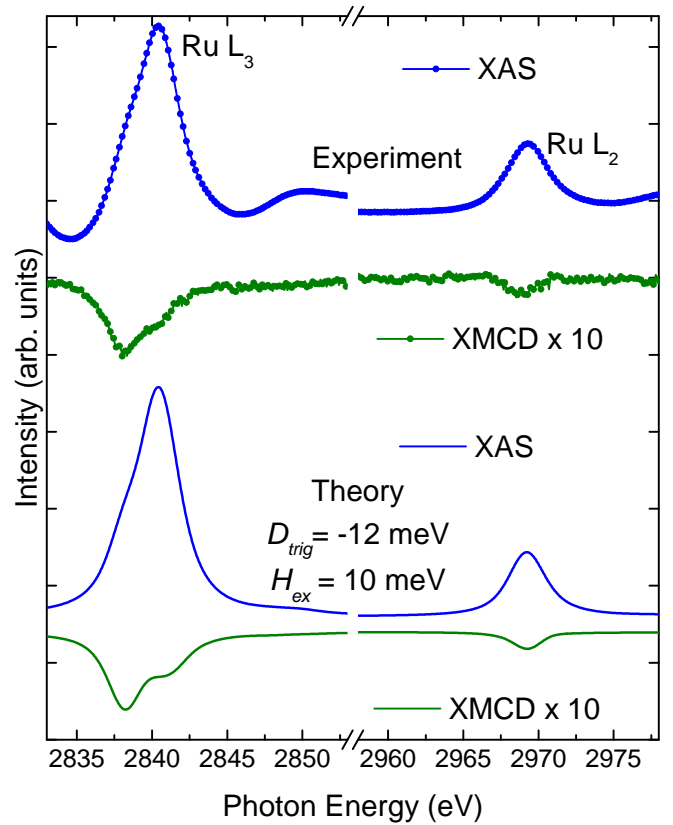


FIG. 5: (color online) Experimental $\text{Ru-}L_{2,3}$ XAS (blue circles) and XMCD (green circles) spectra of a RuCl_3 single crystal together with calculated XAS (blue line) and XMCD (green line). The spectra were measured at $T = 2$ K and $B = 6$ T.

sequence of the reduction of the orbital moment from its atomic value when the transition metal ion is placed in a solid. The fact that the XMCD does not change sign clearly indicates that the orbital moment of the Ru^{3+} ion in RuCl_3 is large, possibly close to the atomic values. From our configuration-interaction calculations we obtain a ratio of $L_x/2S_x = 2.0$ for $H_{ex} = 10$ meV (2.1 if $H_{ex} = 0$ meV). This value is very close to the ratio between the orbital and the spin moments expected for a pure $J_{eff} = 1/2$ system [43].

From the Zeeman splitting of the energy levels in the presence of an applied magnetic field we can calculate the magnetic g factor to be $g_x = g_y = 2.27$ and $g_z = 2.05$ [44]. The fairly isotropic g factor ($g_x/g_z = 1.1$) indicates that the strong anisotropy shown by both susceptibility [15, 16] and high-field magnetization [14, 15] can not be ascribed to single ion physics. Instead, hybridization with neighboring Ru ions needs to be considered explicitly, giving rise to various nearest neighbor and next nearest neighbor Heisenberg, Kitaev and off-diagonal couplings [22]. Our calculations also shows that the average $g = (2g_x + g_z)/3 = 2.2$ is larger than that (2.0) for a pure ionic t_{2g}^5 system. While covalency tends to de-

crease the value of the g factor, the mixing-in of some e_g character into the t_{2g} manifold will quickly increase the g factor value. This e_g - t_{2g} mixing can take place locally on a one-electron level, for example by the presence of a trigonal crystal field, but also (and in fact, certainly) on a many-electron level due to the presence of atomic multiplet interactions (Slater F^2 and F^4 integrals) which are not at all small compared to the e_g - t_{2g} crystal field splitting ($10Dq$).

To summarize, our X-ray absorption linear dichroism study demonstrates that the ground state of RuCl_3 is a doublet with a very close to perfect cubic local symmetry. Our excellent simulations of the experimental spectra give a ratio of 2.0 between the orbital and the spin contributions to the local Ru $4d$ magnetic moment, i.e. the value expected for a $J_{\text{eff}} = 1/2$ ground state. Further quantitative modeling is highly desired as to include not only the Ru t_{2g} but also the e_g orbitals.

We would like to thank the NSRRC and ALBA for providing us with beam time and for the support from the staff during the experiments. The research in Dresden was partially supported by the Deutsche Forschungsgemeinschaft through SFB 1143 and FOR1346. K.-T. Ko acknowledges support from the Max Planck-POSTECH Center for Complex Phase Materials (No. KR2011-0031558).

-
- [1] Y. Singh, S. Manni, J. Reuther, T. Berlijn, R. Thomale, W. Ku, S. Trebst, and P. Gegenwart, Phys. Rev. Lett. **108**, 127203 (2012).
- [2] J. Chaloupka, G. Jackeli, and G. Khaliullin, Phys. Rev. Lett. **105**, 027204 (2010).
- [3] J. Reuther, R. Thomale, and S. Trebst, Phys. Rev. B **84**, 100406 (2011).
- [4] A. Kitaev, Ann. Phys. **321**, 2 (2006).
- [5] Y. Singh and P. Gegenwart, Phys. Rev. B **82**, 064412 (2010).
- [6] H. Gretarsson, J. P. Clancy, X. Liu, J. P. Hill, Emil Bozin, Yogesh Singh, S. Manni, P. Gegenwart, Jung-ho Kim, A. H. Said, D. Casa, T. Gog, M. H. Upton, Heung-Sik Kim, J. Yu, Vamshi M. Katukuri, L. Hozoi, Jeroen van den Brink, and Young-June Kim, Phys. Rev. Lett. **110**, 076402 (2013).
- [7] I. I. Mazin, Harald O. Jeschke, Kateryna Foyevtsova, Roser Valentí, and D. I. Khomskii, Phys. Rev. Lett. **109**, 197201 (2012).
- [8] Kateryna Foyevtsova, Harald O. Jeschke, I. I. Mazin, D. I. Khomskii, and Roser Valentí, Phys. Rev. B **88**, 035107 (2013).
- [9] S. Agrestini, C.-Y. Kuo, M. Moretti Sala, Z. Hu, D. Kasinathan, K.-T. Ko, P. Glatzel, M. Rossi, J.-D. Cafun, K. O. Kvashnina, A. Matsumoto, T. Takayama, H. Takagi, L. H. Tjeng, and M. W. Haverkort, arXiv:1612.00074
- [10] K. W. Plumb, J. P. Clancy, L. J. Sandilands, V. V. Shankar, Y. F. Hu, K. S. Burch, Hae-Young Kee, and Young-June Kim, Phys. Rev. B **90**, 041112(R) (2014).
- [11] Luke J. Sandilands, Yao Tian, Kemp W. Plumb, and Young-June Kim, Kenneth S. Burch, Phys. Rev. Lett. **114**, 147201 (2015).
- [12] J. Nasu, J. Knolle, D. L. Kovrizhin, Y. Motome and R. Moessner, Nat. Phys. **12**, 912 (2016).
- [13] A. Banerjee, C. A. Bridges, J.-Q. Yan, A. A. Aczel, L. Li, M. B. Stone, G. E. Granroth, M. D. Lumsden, Y. Yiu, J. Knolle, S. Bhattacharjee, D. L. Kovrizhin, R. Moessner, D. A. Tennant, D. G. Mandrus, and S. E. Nagler, Nature Materials **15**, 733 (2016).
- [14] R. D. Johnson, S. C. Williams, A. A. Haghighirad, J. Singleton, V. Zapf, P. Manuel, I. I. Mazin, Y. Li, H. O. Jeschke, R. Valentí, and R. Coldea, Phys. Rev. B **92**, 235119 (2015).
- [15] Yumi Kubota, Hidekazu Tanaka, Toshio Ono, Yasuo Narumi, and Koichi Kindo, Phys. Rev. B **91**, 094422 (2015).
- [16] M. Majumder, M. Schmidt, H. Rosner, A. A. Tsirlin, H. Yasuoka, and M. Baenitz, Phys. Rev. B **91**, 180401(R) (2015).
- [17] Heung-Sik Kim, Vijay Shankar V., Andrei Catuneanu, and Hae-Young Kee, Phys. Rev. B **91**, 241110(R) (2015).
- [18] I. Rousochatzakis, J. Reuther, R. Thomale, S. Rachel, and N. B. Perkins, Phys. Rev. X **5**, 041035 (2015).
- [19] H. B. Cao, A. Banerjee, J.-Q. Yan, C. A. Bridges, M. D. Lumsden, D. G. Mandrus, D. A. Tennant, B. C. Chakoumakos, and S. E. Nagler, Phys. Rev. B **93**, 134423 (2016).
- [20] Ravi Yadav, Nikolay A. Bogdanov, Vamshi M. Katukuri, Satoshi Nishimoto, Jeroen van den Brink, and Liviu Hozoi, Scientific Report **6**, 37925 (2016).
- [21] Luke J. Sandilands, Yao Tian, Anjan A. Reijnders, Heung-Sik Kim, K. W. Plumb, and Young-June Kim, Hae-Young Kee, and Kenneth S. Burch, Phys. Rev. B **93**, 075144 (2016).
- [22] Stephen M. Winter, Ying Li, Harald O. Jeschke, and Roser Valentí, Phys. Rev. B **93**, 214431 (2016).
- [23] J. Chaloupka and G. Khaliullin, Phys. Rev. B **94**, 064435 (2016).
- [24] Heung-Sik Kim and Hae-Young Kee, Phys. Rev. B **93**, 155143 (2016).
- [25] F. Lang, P. J. Baker, A. A. Haghighirad, Y. Li, D. Prabhakaran, R. Valentí, and S. J. Blundell, Phys. Rev. B **94**, 020407(R) (2016).
- [26] A. Koitzsch, C. Habenicht, E. Müller, M. Knupfer, B. Büchner, H. C. Kandpal, J. van den Brink, D. Nowak, A. Isaeva, and Th. Doert, Phys. Rev. Lett. **117**, 126403 (2016).
- [27] L. Janssen, E. C. Andrade, and M. Vojta, Phys. Rev. Lett. **117**, 277202 (2016).
- [28] Y. Sizyuk, P. Wölfle, and N. B. Perkins, Phys. Rev. B **94**, 085109 (2016).
- [29] Xiaoqing Zhou, Haoxiang Li, J. A. Waugh, S. Parham, Heung-Sik Kim, J. A. Sears, A. Gomes, Hae-Young Kee, Young-June Kim, and D. S. Dessau, Phys. Rev. B **94**, 161106(R) (2016).
- [30] M. Ziatdinov, A. Banerjee, A. Maksov, T. Berlijn, W. Zhou, H.B. Cao, J.-Q. Yan, C.A. Bridges, D.G. Mandrus, S.E. Nagler, A.P. Baddorf, and S.V. Kalinin, Nat. Comm. **7**, 13774 (2016).
- [31] J. A. Sears, M. Songvilay, K. W. Plumb, J. P. Clancy, Y. Qiu, Y. Zhao, D. Parshall, and Young-June Kim, Phys. Rev. B **91**, 144420 (2015).
- [32] Soobin Sinn, Choong Hyun Kim, Beom Hyun Kim, Kyung Dong Lee, Choong Jae Won, Ji Seop Oh, Moon-

- sup Han, Young Jun Chang, Namjung Hur, Hitoshi Sato, Byeong-Gyu Park, Changyoung Kim, Hyeong-Do Kim, and Tae Won Noh, Scientific Report **6**, 39544 (2016).
- [33] Kejing Ran, Jinghui Wang, Wei Wang, Zhao-Yang Dong, Xiao Ren, Song Bao, Shichao Li, Zhen Ma, Yuan Gan, Youtian Zhang, J. T. Park, Guochu Deng, S. Danilkin, Shun-Li Yu, Jian-Xin Li, and Jinsheng Wen, Phys. Rev. Lett. **118**, 107203 (2017).
- [34] Andrei Catuneanu, Heung-Sik Kim, Oguzhan Can, and Hae-Young Kee, Phys. Rev. B **94**, 121118(R) (2016).
- [35] Luke J. Sandilands, C. H. Sohn, H. J. Park, So Yeun Kim, K. W. Kim, Jennifer A. Sears, Young-June Kim, and Tae Won Noh, Phys. Rev. B **94**, 195156 (2016).
- [36] E. V. Stroganov and K. V. Ovchinnikov, Ser. Fiz. i Khim. **12**, 152 (1957).
- [37] K. Koepernik, and H. Eschrig, Phys. Rev. B **59**, 1743 (1999).
- [38] The Coulomb repulsion U was set to 1.5 eV and the Hund's exchange to 0.3 eV, following Refs. 10, 16.
- [39] See the "Theo Thole Memorial Issue", J. Electron. Spectrosc. Relat. Phenom. **86**, 1 (1997).
- [40] F. de Groot, J. Electron Spectrosc. Relat. Phenom. **67**, 529 (1994).
- [41] A. Tanaka and T. Jo, J. Phys. Soc. Jpn. **63**, 2788 (1994).
- [42] $U_{dd} = 4.0$ eV, $U_{pd} = 5.5$ eV, charge transfer energy $\Delta_{CT} = 5.0$ eV, SOC = 0.15 eV, ionic crystal field $10Dq^{ion} = 1.5$ eV, $D_{trig}^{ion} = -12.0$ meV, hybridization $V(e_g^\sigma) = 3.336$ eV, $V(e_g^\pi) = V(a_{1g}) = 1.76$ eV, ligand crystal field $10Dq^{lig} = 1.3$ eV. Slater integrals were reduced to 70 % of the Hartree-Fock values. The effective cubic crystal field is $10Dq^{eff} = 2.35$ eV. Gaussian (0.4 eV for the XAS in Fig. 3 and 1.4 eV for the XAS in Fig. 5) and Lorentzian (2 eV) broadenings were applied in order to take into account experimental resolution and lifetime effects, respectively.
- [43] B. J. Kim, H. Jin, S. J. Moon, J. Y. Kim, B. G. Park, C. S. Leem, J. Yu, T. W. Noh, C. Kim, S. J. Oh, J. H. Park, V. Durairaj, G. Cao, and E. Rotenberg, Phys. Rev. Lett. **101**, 076402 (2008).
- [44] In our estimation of the g factor we considered $H_{ex} = 0$ meV.

Electronically highly cubic conditions for Ru in α -RuCl₃

S. Agrestini,⁵ C.-Y. Kuo,⁵ K.-T. Ko,⁵ Z. Hu,⁵ D. Kasinathan,⁵ H. Babu Vasili,⁶ J. Herrero-Martin,⁶ S. M. Valvidares,⁶ E. Pellegrin,⁶ L.-Y. Jang,⁷ A. Henschel,⁵ M. Schmidt,⁵ A. Tanaka,⁸ and L. H. Tjeng⁵

⁵Max Planck Institute for Chemical Physics of Solids, Nöthnitzerstr. 40, 01187 Dresden, Germany

⁶ALBA Synchrotron Light Source, E-08290 Cerdanyola del Vallès, Barcelona, Spain

⁷National Synchrotron Radiation Research Center, 101 Hsin-Ann Road, Hsinchu 30076, Taiwan

⁸Department of Quantum Matter, ADSM, Hiroshima University, Higashi-Hiroshima 739-8530, Japan

(Dated: June 3, 2021)

PACS numbers: 71.70.Ch, 75.70.Tj, 75.10.Kt, 78.70.Dm, 72.80.Ga

In Fig. S1 we report simulations for the Ru- $L_{2,3}$ XCMD spectra calculated for $T = 2$ K and $B = 6$ T using different values of the trigonal crystal field splitting D_{trig} under the assumption that the exchange field H_{ex} is absent. One can clearly observe that the simulated XCMD signal is always much larger than the measured one of RuCl₃, no matter what trigonal distortion is considered.

In Fig. S2 we show the simulations for the XCMD for different values of H_{ex} with D_{trig} fixed at -12 meV. The exchange field has a very strong influence on the magnitude of the XCMD signal. The experimental XCMD is best simulated for $H_{ex} = 10$ meV. We note that in the considered range, the exchange field has no significant effect on the lineshape of the XCMD spectrum but determines mainly the size of the XCMD signal.

Fig. S3 displays the simulations for the XCMD as a function of D_{trig} in order to investigate the sensitivity of the XCMD lineshape to D_{trig} . The calculations have been done for a fixed $H_{ex} = 10$ meV and the curves have been normalized to the XCMD peak height to highlight the lineshape of the spectra rather than the magnitude

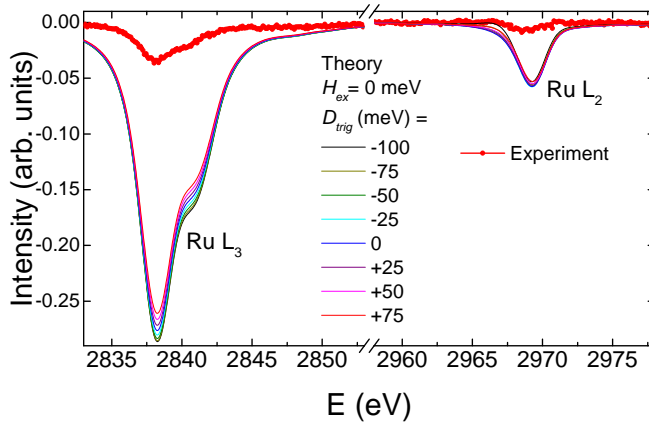


FIG. S1: (color online) Ru- $L_{2,3}$ XCMD simulations (solid lines) calculated using different values of the trigonal crystal field splitting D_{trig} with the exchange field H_{ex} set to zero. The calculations were done for $T = 2$ K and $B = 6$ T, the conditions at which the experimental XCMD spectrum of RuCl₃ was taken (red circles). The intensity was normalized to have the calculated Ru- L_3 XAS peak height to match the experimental one.

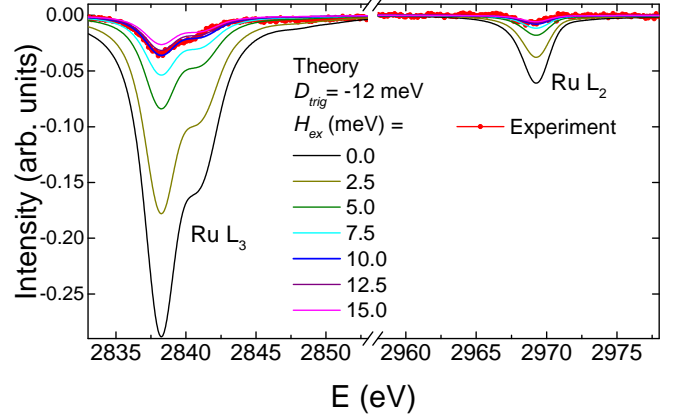


FIG. S2: (color online) Ru- $L_{2,3}$ XCMD simulations (solid lines) calculated using different values of H_{ex} with D_{trig} set at -12 meV. The experimental XCMD spectrum of RuCl₃ is also given (red circles). The intensity was normalized to have the calculated Ru- L_3 XAS peak height to match the experimental one.

of the signal. The top panel shows the results for a large range of D_{trig} , i.e. between -500 and +500 meV, and the bottom panel presents the result for a narrower range with smaller steps, i.e. between -100 and +100 meV. From the figure we can observe that the spectral lineshape of XCMD is sensitive to the trigonal crystal field splitting, but only so if the D_{trig} value is varied in a range that exceeds the spin-orbit coupling constant of about 150 meV. Varying D_{trig} between -50 and +100 meV in fact does not change the lineshape visibly. In other words, XCMD alone is not a very sensitive method to determine D_{trig} accurately. To establish whether the $J_{eff} = 1/2$ condition is fulfilled (or not) implies that one needs to determine whether D_{trig} is negligible (or not negligible) compared to the spin-orbit constant. The more accurate method to resolve this issue is to measure the smallness of the linear dichroism in the XAS itself. XCMD is valuable to determine the magnitude of the exchange field and to serve as a strict consistency check of the simulations: the same set of parameters must provide excellent simulations for both the XAS and the XCMD spectra.

In literature the sum rules for XCMD developed by

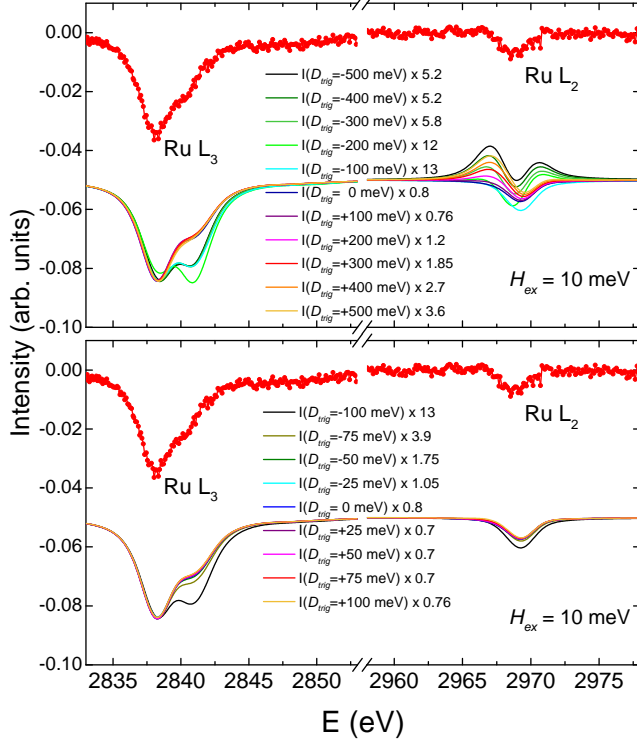


FIG. S3: (color online) Ru- $L_{2,3}$ XMCD simulations (solid lines) calculated using different values of D_{trig} with $H_{ex} = 10$ meV, together with the experimental XMCD spectrum of RuCl₃ (red circles). In the top panel D_{trig} is varied between -500 and +500 meV, and in the bottom panel between -100 and +100 meV. For a better comparison of the line shapes, the simulated spectra are normalized to the XMCD peak height, with the normalization factor also indicated in the legend.

Thole and Carra et al. [1, 2] are often used to extract directly from the spectrum the ratio of orbital and spin moments. The sum rules can be summarized as:

$$\frac{L_x}{2S_x + 7T_x} = \frac{2}{3} \cdot \frac{\int_{L_{2,3}} (\sigma^+ - \sigma^-) dE}{\int_{L_3} (\sigma^+ - \sigma^-) dE - 2 \int_{L_2} (\sigma^+ - \sigma^-) dE} \quad (1)$$

where S_x and L_x are the spin and orbital contributions to the local magnetic moment, respectively, and T_x is the intra-atomic magnetic dipole moment. The application of the sum rules to our experimental Ru $L_{2,3}$ XMCD data gives $L_x/(2S_x + 7T_x) = 1.0(1)$, which confirms that the orbital moment of Ru³⁺ is relatively large. If we use the value of $T_x/2S_x = 0.15$ given by our configuration-interaction calculations, we obtain from the application of the sum rules the ratio $L_x/2S_x = 2.0(1)$, which is in very good agreement with the value given by our configuration interaction calculations for $D_{trig} = 5$ meV and $H_{ex} = 10$ meV. This demonstrates that the analysis using the sum rules is fully consistent with the analysis based on the simulations of the XAS and XMCD spectra, i.e.

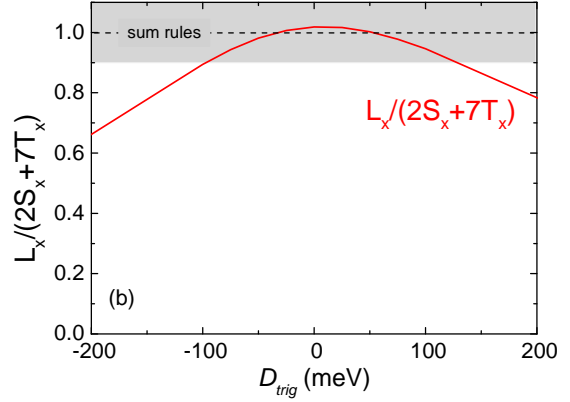


FIG. S4: (color online) Calculated $L_x/(2S_x + 7T_x)$ for $H_{ex} = 10$ meV as a function of D_{trig} . The horizontal dashed line indicates the $L_x/(2S_x + 7T_x)$ value given by the sum rules applied to the experimental XMCD data and the shadow area represents its error bar.

analyses based on the lineshape, as it should be.

Fig. S4 shows the calculated $L_x/(2S_x + 7T_x)$ ratio as a function of the trigonal crystal field splitting for a fixed exchange field of 10 meV. We can clearly observe that the sum rule quantity $L_x/(2S_x + 7T_x)$ is a slowly varying function of D_{trig} . The experimental XMCD data is given by the dashed line and the shadow area represents its error bar. Hence, the value obtained by applying the sum rules to the XMCD data can correspond to the wide range $-100 \leq D_{trig} \leq +100$ meV. In other words, our calculations reveal that the XMCD alone of RuCl₃ cannot, either through spectral lineshape analysis or through the application of the sum rules, provide a value of D_{trig} with the required precision. A reliable and accurate determination of D_{trig} can be best obtained from the linear dichroic signal in the polarization dependent XAS spectra as we have reported in the main text of the manuscript.

We would like to note that in our model we have taken into account the zig-zag modulated magnetic structure (shown in fig. 3) proposed by Cao et al. [3], by applying an exchange field of 10 meV along the direction of the Ru spins, which forms an angle of $\phi = 35^\circ$ with the ab plane. If the alternative $\phi = -35^\circ$ zig-zag magnetic structure is considered then the exchange field has to be reduced to 3 meV in order to simulate the size of the experimental XMCD signal. The reason of the need of reducing the exchange field lies in the fact that in the case of the second magnetic structure the applied magnetic field would be close to the direction of the spins, which is a hard direction for the magnetization. With the present XMCD data we are not able to distinguish which of the two magnetic structure is correct. Yet, this does not affect the conclusions that we have made about the trigonal crystal field value and the $L_x/2S_x = 2.0$ for

RuCl₃, i.e. our finding that the Ru ground state fulfills the $J_{eff} = 1/2$ condition is robust.



- [1] B. T. Thole, P. Carra, F. Sette, and G. van der Laan, Phys. Rev. Lett. **68**, 1943 (1992).
- [2] P. Carra, B. T. Thole, M. Altarelli, and X. Wang, Phys. Rev. Lett. **70**, 694 (1993).
- [3] H. B. Cao, A. Banerjee, J.-Q. Yan, C. A. Bridges, M. D. Lumsden, D. G. Mandrus, D. A. Tennant, B. C. Chakoumakos, and S. E. Nagler, Phys. Rev. B **93**, 134423 (2016).